Electronic Supplementary Material

Optimising hydrogen production via solar acetic acid photoreforming on Cu/TiO_2

Mikel Imizcoz, Alberto V. Puga

S1 Materials

Titanium dioxide (Aeroxide® TiO2 P25) was sourced by Evonik. Hydrogen hexachloroplatinate(IV) hydrate (≥ 99.9% free of trace metals), hydrogen tetrachloroaurate(III) trihydrate (≥ 99.9% free of trace metals), silver nitrate (> 99%), copper(II) nitrate hemi(pentahydrate) (98%) and acetic acid (≥ 99.8%) were supplied by Sigma-Aldrich and used as received. Methanol (reagent grade, ≥ 99.9%) was supplied by Scharlau and used as received. Ultra-pure water was obtained using a Milli-Q® purification system. Argon (≥ 99.995%) and synthetic air (79% N_2, 21% O_2) were supplied by Abelló Linde.

S2 Synthesis of photocatalysts

The *M*(*X*%)/TiO_2 (*M* = Pt, Au, Ag or Cu; X: nominal *M*/TiO_2 %wt loading) photocatalysts used in this work were prepared by the photodeposition method. In a typical procedure, TiO_2 (200 mg) was dispersed in ultra-pure water (25 mL) containing the desired amounts of metallic precursor and methanol, as detailed in Table S1. The suspensions were sonicated for 10 min and then transferred to cylindrical quartz cells (diameter ≈ 44 mm, volume ≈ 50 mL, equipped with a gas inlet valve, a gas outlet valve and a pressure gauge). The cells were evacuated under vacuum (≈ 10 mbar, 2 min) and then purged with argon (pressurising up to 2 bar and depressurising, five cycles). The cells were loaded with argon (1.5 bar) and the stirred (500 min^{-1}) suspensions irradiated under UV-vis light from a mercury lamp (125 W, irradiance ≈ 1.5 kW m^{-2}, measured employing a calibrated photodiode) for 3 h. The suspensions turned from off-white to intense colours at the end of the photodeposition processes. The solids were separated by filtration using polyamide membrane filters (Whatman®, pore size = 0.45 μm), washed with ultra-pure water (*ca*. 0.3 L) and dried under a stream of air by suction. The resulting pastes were further dried under vacuum (≈ 10 mbar) at room temperature until constant weight to obtain the final *M*(*X*%)/TiO_2 photocatalysts (Table S1). Images of the suspensions during preparation, of the isolated solid, and of the re-suspension in CH_3COOH/H_2O are shown in Fig. S7.

Table S1 Synthetic details for the preparation of *M*(*X*%)/TiO_2 (*M* = Pt, Au, Ag or Cu; *X*: nominal *M*/TiO_2 %*wt* loading) photocatalysts.

photocatalyst	metallic precursor	methanol amount/mg	colour
Pt(1%)/TiO_2	$H_2Cl_6Pt{\cdot}6H_2O$	80	grey
Au(1%)/TiO_2	$HAuCl_4{\cdot}3H_2O$	80	purple
Ag(1%)/TiO_2	$AgNO_3$	80	purple
Cu(1%)/TiO_2	$Cu(NO_3)_2{\cdot}{}^5/_2H_2O$	80	pale blue
Cu(3%)/TiO_2	$Cu(NO_3)_2{\cdot}{}^5/_2H_2O$	236	pale blue
Cu(10%)/TiO_2	$Cu(NO_3)_2{\cdot}{}^5/_2H_2O$	780	grey-blue

S3 Photocatalyst characterisations

Metallic contents were determined by inductively coupled plasma (ICP) analyses performed on a Varian 715-ES ICP Optical Emission Spectrometer after dissolution of the samples in aqueous HF/HNO_3/HCl (1:1:3) mixtures. In the case of silver, ICP did not provide satisfactory results due to the formation of precipitates or deposits during dissolution, and therefore, elemental analyses were performed by means of field emission scanning electron microscopy coupled to energy dispersive X-ray spectroscopy (FESEM-EDX) on a JEOL 7001F microscope equipped with an Oxford Instruments detector, after depositing a layer of powdered sample on carbon tape; elemental percentages were averaged over a number of measurements on different areas of the specimen. X-ray diffraction (XRD) measurements were performed by means of a PANalytical Cubix'Pro diffractometer equipped with an X'Celerator detector and automatic divergence and reception slits using Cu-K_α radiation (0.154056 nm). The mean size of the ordered (crystalline) domains (ø) was estimated using the Scherrer equation. Transmission electron microscopy (TEM) images were taken on JEOL 2100F microscope operating at 200 kV both in high-resolution transmission (HRTEM) and scanning-transmission (STEM) modes, coupled with an Inca Energy TEM 200 (Oxford) energy dispersive X-ray (EDX) spectroscope for elemental analyses. STEM images were obtained using a High Angle Annular Dark Field (HAADF) detector, which allows Z-contrast imaging. Samples were deposited on carbon-coated nickel grids. The sizes of metal co-catalyst nanoparticles and standard deviations were calculated by determining diameters for a minimum of forty particles in STEM images by using the Image J software. UV-vis absorption spectra were recorded by diffuse reflectance UV-vis (DRUV-vis) spectroscopy on a Varian Cary 5000 UV-Vis-NIR Spectrophotometer. X-ray photoelectron spectroscopy (XPS) data were collected on a SPECS spectrometer equipped with a 150-MCD-9 detector and using a non-monochromatic Al-K_α (1486.6 eV) X-ray source. Spectra were recorded at room temperature, using an analyser pass energy of 30 eV, an X-ray power of 50 W and under an operating pressure of 10^{-9} mbar. During data processing of the XPS spectra, binding energy (BE) values were referenced to the C1s signal (284.5 eV). Spectra treatment was performed using the CASA software.

S4 Photocatalytic reactions

S4.1 *Conventional procedure*. In a typical experiment, the photocatalyst powder (25 mg) was suspended in a CH_3COOH/H_2O mixture (1:1 by volume, 25 mL) by sonication for 10 min. The resulting suspension was then transferred to a cylindrical quartz reactor (see details in Section S2). The cell was evacuated under vacuum (≈ 10 mbar, 2 min) and then purged with argon (pressurising up to 2 bar and depressurising for five cycles), and finally loaded with argon (1.5 bar). The suspension was stirred (500 min^{-1}) and irradiated using a solar simulator (ThermoOriel 91192-1000, equipped with a 1000 W Xe lamp and an AM1.5G filter to simulate the spectrum of sunlight; irradiance≈ 1.0 kW m^{-2}). Gas phase samples (2 cm^3) were taken and analysed on a two-channel chromatograph (Agilent 490 Micro GC, carrier gas: Ar) equipped with thermal conductivity detectors (TCD), and a MS 5 Å column (first channel) for the quantification of H_2, and a PoraPLOT Q column (second channel) for the quantification of CH_4, CO_2 and C_2H_6.

S4.2 *Procedure using in situ photodeposited photocatalysts*. The photocatalytic experiments performed using *in situ* photodeposited $Cu(3\%)/TiO_2$ ($^{IS}Cu(3\%)/TiO_2$) were carried out by directly irradiating a stirred (500 min^{-1}) suspension of TiO_2 (24.3 mg) in a CH_3COOH/H_2O mixture (1:1 by volume, 25 mL) containing the appropriate amount of $Cu(NO_3)_2{\cdot}^5/_2H_2O$ (2.7 mg, 3% Cu relative to TiO_2 by weight) under UV-vis light from a mercury lamp (125 W, irradiance ≈ 1.5 kW m^{-2}) for 3 h, in an analogous fashion to the synthetic procedure described above (S4.1). The suspension was deep purple at the end of this photodeposition process. The cell was then evacuated under vacuum (≈ 10 mbar, 2 min), purged, pressurised with argon, and ultimately irradiated under simulated sunlight in a similar way to the conventional procedure described in Section S4.1 above.

S4.3 *Procedure under monochromatic light for photonic efficiency determination*. A suspension of $^{IS}Cu(3\%)/TiO_2$, prepared as described in Section S4.2 above. The resulted purple suspension was irradiated under light at 350 nm by using a Czerny-Turner-type Microbeam monochromator equipped with a 150 W Xe lamp, and powered by a Pluton Technology International LPS 220B power supply. Irradiances were measured employing a calibrated photodiode.

S4.4 *Redox cycling procedure*. In order to study the effect of the oxidation state of copper on the selectivity of the solar photocatalytic transformation of aqueous acetic acid, redox cycling experiments were performed by photoreduction under UV-vis irradiation or deliberate oxidation under air, as detailed herein. The initial cycle (*#ox1*) was performed as for the conventional procedure described above, using $Cu(3\%)/TiO_2$ (25.0 mg, comprising mainly oxidised copper species as the co-catalyst, see main text for discussion), and a CH_3COOH/H_2O mixture (1:1 by volume, 25 mL), under simulated sunlight irradiation (AM1.5G, irradiance≈ 1.0 kW m^{-2}) for 3 h. The second cycle (*#red1*) was performed after a photoreduction treatment of the reaction suspension by evacuating the gaseous headspace of the cell (≈ 10 mbar, 5 min), refilling with Ar (1.5 bar) and irradiating the suspension under

UV-vis (Hg lamp, 125 W, irradiance ≈ 1.5 kW m^{-2}) for 3 h, whereby the suspension turned into a bright purple-pink colour. Then, the solar irradiation process was carried out as detailed above during the #*ox1* cycle. The third cycle (#*ox2*) was done after deliberate oxidation under synthetic air flow (bubbling at 5 mL min^{-1}, 1 h), until the purple-pink colour of the suspension faded to off-white. Then, the solar irradiation process was carried out as for the previous cycles. The final cycle (#*red2*) was carried out after another photoreduction procedure identical to that used before the #red1 cycle, also resulting in a bright purple-pink suspension. Images of the suspensions, and related results of the photocatalytic reactions are displayed in Fig. 4.

Table S2 Metallic loading for the *M*(*X*%)/TiO_2 photocatalysts relative to the experimentally measured amount of TiO_2, as determined by either ICP or FESEM-EDX.

photocatalyst	loading(*M*)/%	standard deviation/%	method
Pt(1%)/TiO_2	0.87	-	ICP
Au(1%)/TiO_2	1.06	-	ICP
Ag(1%)/TiO_2	1.38	0.35	FESEM-EDX
Cu(1%)/TiO_2	0.97	-	ICP
Cu(3%)/TiO_2	3.18	-	ICP
Cu(10%)/TiO_2	11.11	-	ICP

Table S3 Amounts of gaseous products formed upon short-time simulated sunlight irradiation of aqueous acetic acid using *M*(1%)/TiO_2 photocatalysts.[a]

M	produced amounts/µmol				H_2/CH_4
	H_2	CH_4	CO_2	C_2H_6	
none	0.7	11.8	7.0	< 0.1	0.06
Pt	33.5	84.0	45.7	0.9	0.40
Au	0.6	14.1	8.7	0.2	0.04
Ag	0.2	14.1	8.2	< 0.1	0.01
Cu	< 0.1	97.6	48.1	0.2	< 0.01
Cu (dark)[b]	-	-	-	-	-

[a] Reaction conditions: CH_3COOH/H_2O (1:1 *v*/*v*, 25 mL), suspended *M*/TiO_2 (25 mg), simulated sunlight irradiation (AM1.5G, 100 mW cm^{-2}), *t* = 2 h. [b] Reaction performed using identical conditions as for the other entries, but in the absence of irradiation.

Table S4 Comparison of literature data and data from this work on the photocatalytic transformation of acetic acid (plus formic acid to extend the scope to the simplest carboxylic acid) in irradiated aqueous suspensions of Cu/TiO_2 and related photocatalysts. Since literature data on Cu/TiO_2 is scarce and only related to irradiations under UV-rich light (e.g. from Hg lamps), only a qualitative comparison to the systems reported in this work can be done. Literature data using other metal co-catalysts in similar photocatalytic systems can be found and are listed below, showing that the performance is similar for Pt, Au or Ag, and that H_2 selectivity is in general moderate due to the prevalence of decarboxylation unless basic media are employed.

						production rates/μmol g_{cat}^{-1} h^{-1}				
photocatalyst	co-catalyst deposition method	reaction medium	light source	*P*/W or (*I*/mW cm^{-2})	*T*/°C	H_2	CO_2	CH_4	C_2H_6	reference
Cu/TiO_2(anatase)	Cu^{2+} in reaction medium	HCOOH (*aq*, 1 M)[a]	UV	125	25	2500[b]	-	-	-	1
Pt(0.5%)/Cu_2O	photodeposition	HCOOH (*aq*, 2.5 M, pH 5)[c]	halogen (> 420 nm)	(280)	-	155	158	-	-	2
Cu_2O	-	HCOOH (*aq*, 2.5 M, pH 5)[c]	halogen (> 420 nm)	(280)	-	65	64	-	-	2
Cu(10%)/TiO_2	mechanical mixing	CH_3COOH (*aq*, 1 M)	Hg	-	25	144	640	590	66	3
CuO(33.3%)-SnO_2	precipitation-calcination	CH_3COOH (*aq*, 0.04 M)	Hg	300	45	6473[b]				4
CuO(33.3%)-SnO_2	precipitation-calcination	CH_3COOH (*aq*, 0.04 M)	Hg	300	45	17904[b]				4
Pt(7%)/TiO_2(rutile)	photodeposition	H_2O/CH_3COOH (*l*, 6:1, pH 2.1)[c]	Xe (> 320 nm)	500	-	77	-	397	-	5
Pt(7%)/TiO_2(rutile)	photodeposition	H_2O/ CH_3COOH (*l*, 6:1, pH 8.8)[c]	Xe (> 320 nm)	500	-	367	-	2	-	5
Pt(7%)/TiO_2(anatase)	photodeposition	$Na[CH_3COO]$ (*aq*, 1.7% w/v, pH = 7.4)[c]	Xe (> 320 nm)	500	-	165	27	0.24	-	5
Pt(0.5%)/TiO_2(P25)	impregnation-reduction	CH_3COOH (*aq*, 0.87 mM)	solar simulator	280	40	278[b]	-	-	-	6
Pt(1%)/TiO_2(P25)	impregnation-sonication	CH_3COOH (*aq*, 0.5 M, pH = 2)[d]	Xe	1000	25	440	1280	640	26	7
Pt(1%)/TiO_2(P25)	impregnation-sonication	CH_3COOH (*aq*, 0.5 M, pH = 11)[c]	Xe	1000	25	100	-	0.200	0.016	7
photocatalyst	co-catalyst	reaction medium	light source	(*I*/mW cm^{-2})	*T*/°C	H_2	CO_2	CH_4	C_2H_6	reference

	deposition method									
Pt(1%)/TiO_2(P25)	impregnation-sonication	CH_3COOH (*aq*, 0.5 M, pH = 2)[c]	Xe	1000	25	955	2739	1363	64	8
Rh(1%)/TiO_2(P25)	photodeposition	CH_3COOH (*aq*, 0.5 M, pH = 2)[c]	Xe	1000	25	472	1547	709	35	8
Au(1%)/TiO_2(P25)	photodeposition	CH_3COOH (*aq*, 0.5 M, pH = 2)[c]	Xe	1000	25	307	1331	613	53	8
Ag(1%)/TiO_2(P25)	photodeposition	CH_3COOH (*aq*, 0.5 M, pH = 2)[c]	Xe	1000	25	77	952	672	16	8
IrO_2(1%)/TiO_2(P25)	impregnation-calcination	CH_3COOH (*aq*, 0.5 M, pH = 2)[c]	Xe	1000	25	155	2373	1563	64	8
RuO_2(1%)/TiO_2(P25)	impregnation-calcination	CH_3COOH (*aq*, 0.5 M, pH = 2)[c]	Xe	1000	25	245	1701	744	19	8
TiO_2(P25)	-	H_2O/CH_3COOH, (*l*, 1:1)	solar simulator	(100)	25	14	139	236	< 1	this work
Pt(1%)/TiO_2(P25)	photodeposition	H_2O/CH_3COOH, (*l*, 1:1)	solar simulator	(100)	25	670	914	1680	18	this work
Au(1%)/TiO_2(P25)	photodeposition	H_2O/CH_3COOH, (*l*, 1:1)	solar simulator	(100)	25	12	174	281	4	this work
Ag(1%)/TiO_2(P25)	photodeposition	H_2O/CH_3COOH, (*l*, 1:1)	solar simulator	(100)	25	3	164	282	< 1	this work
Cu(1%)/TiO_2(P25)	photodeposition	H_2O/CH_3COOH, (*l*, 1:1)	solar simulator	(100)	25	< 1	962	1951	4	this work
Cu(1%)/TiO_2(P25)	photodeposition	H_2O/CH_3COOH, (*l*, 1:1)	solar simulator	(100)	25	< 1	962	1951	4	this work
Cu(3%)/TiO_2(P25)	photodeposition	H_2O/CH_3COOH, (*l*, 1:1)	solar simulator	(100)	25	2	796	1595	5	this work
Cu(10%)/TiO_2(P25)	photodeposition	H_2O/CH_3COOH, (*l*, 1:1)	solar simulator	(100)	25	< 1	704	1420	< 1	this work
Cu(3%)/TiO_2(P25)	*in situ* photodeposition	H_2O/CH_3COOH, (*l*, 1:1)	solar simulator	(100)	25	36	249	199	4	this work

[a] The solution also contained $HClO_4$ (pH = 1) and NaCl (1 M). [b] Only H_2 analysed. [c] Sodium hydroxide used to adjust pH. [d] Perchloric acid used to adjust pH. References:

1 V. Lanese, D. Spasiano, R. Marotta, I. Di Somma, L. Lisi, S. Cimino and R. Andreozzi, *Int. J. Hydrogen Energy*, 2013, 38, 9644-9654.
2 S. Kakuta and T. Abe, *ACS Appl. Mater. Interfaces*, 2009, 1, 2707-2710.
3 A. Heciak, A.W. Morawski, B. Grzmil and S. Mozia, *Appl. Catal., B-Environ.*, 2013, 140, 108-114.
4 X.-J. Zheng, Y.-J. Wei, L.-F. Wei, B. Xie and M.-B. Wei, *Int. J. Hydrogen Energy*, 2010, 35, 11709-11718.
5 T. Sakata, T. Kawai and K. Hashimoto, *J. Phys. Chem.*, 1984, 88, 2344-2350.
6 A. Patsoura, D.I. Kondarides and X.E. Verykios, *Catal. Today*, 2007, 124, 94-102.
7 S. Hamid, I. Ivanova, T.H. Jeon, R. Dillert, W.Y. Choi and D.W. Bahnemann, *J. Catal.*, 2017, 349, 128-135.
8 S. Hamid, R. Dillert and D.W. Bahnemann, *J. Phys. Chem. C*, 2018, 122, 12792-12809.

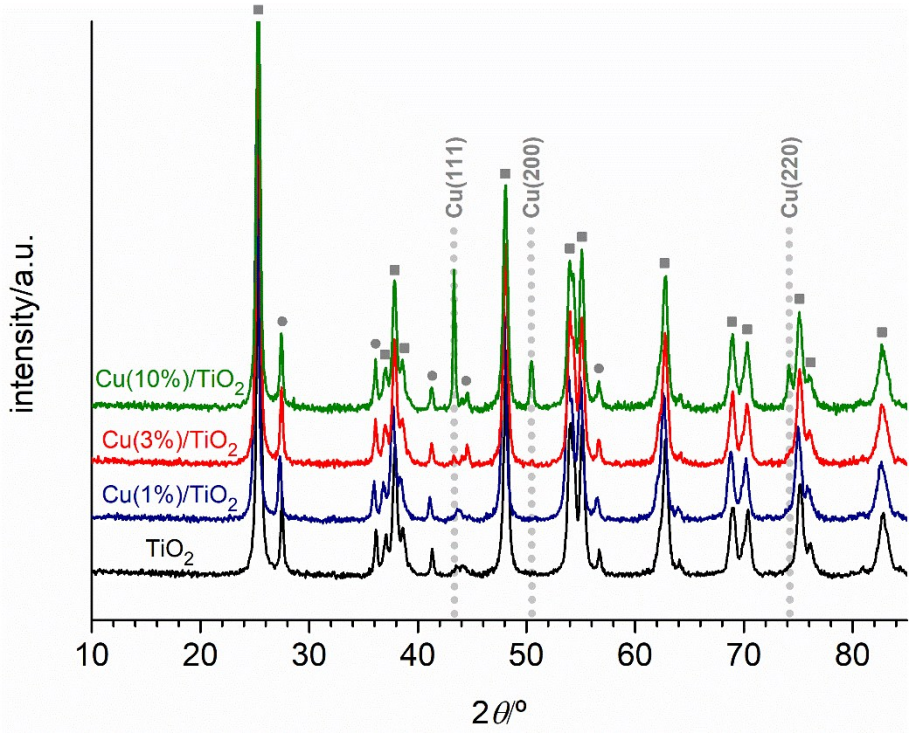

Fig. S1 XRD of the Cu(*X*%)/TiO_2 (*X* = 1, 3 or 10) photocatalysts and of the bare TiO_2. The identified diffraction peaks for metallic copper (face-centred cubic lattice, fcc) are marked by dotted grey lines, and the corresponding planes indicated above them. In any case were diffractions for copper oxide phases observable. In the case of Cu(1%)/TiO_2, neither were Cu(0) diffractions apparent. In contrast, Cu(0) signals could be clearly seen for the materials with higher copper content. For Cu(3%)/TiO_2, these were too weak, but in the case of Cu(10%)/TiO_2, they were strong enough to allow estimation of the particle size according to the Scherrer equation, yielding a value of *ca*. 33 nm. Diffraction peaks corresponding to TiO_2 were identified both for anatase (squares) and rutile (circles) phases.

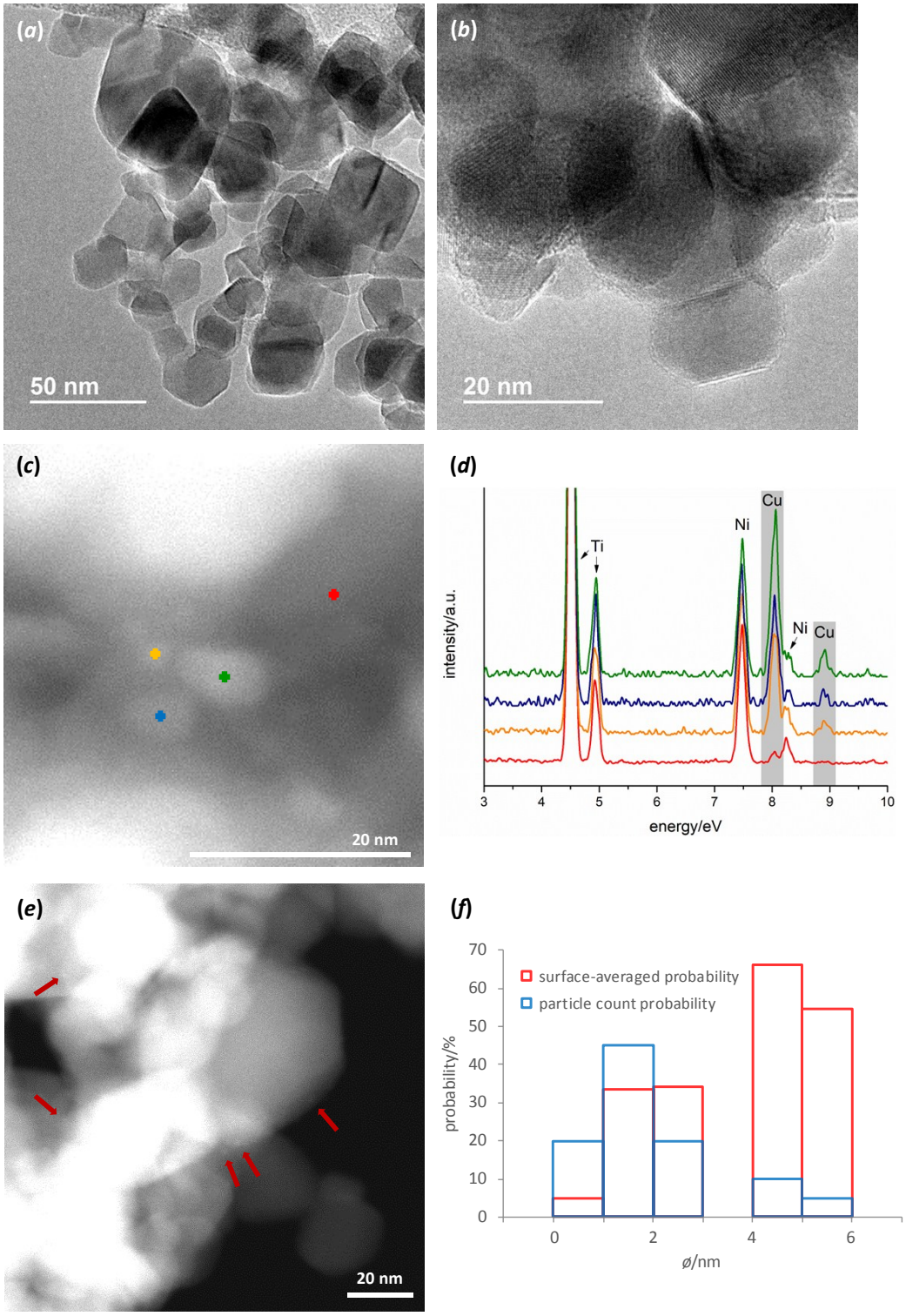

Fig. S2 TEM images and data for Cu(1%)/TiO_2. HRTEM images at × 10^5 and × 3 10^5 magnification (*a* and *b*, respectively) clearly showing the sizes and morphology of the TiO_2 particles, yet not the copper domains, probably due to their small size and the blunt contrast between Cu and Ti. STEM images at high magnification (× 4 10^6 and × 1.2 10^6, *c* and *e*, respectively) showing the presence of small copper particles (marked by arrows in *e*); EDX spectra (*d*) acquired from the points marked in (*c*) confirmed that the smaller (< 6 nm) particles are mainly formed by copper, whereas the larger TiO_2 particles contain negligible amounts of such metal. The particle distribution histogram is represented as histograms both for particle number and surface-averaged probability (*f*).

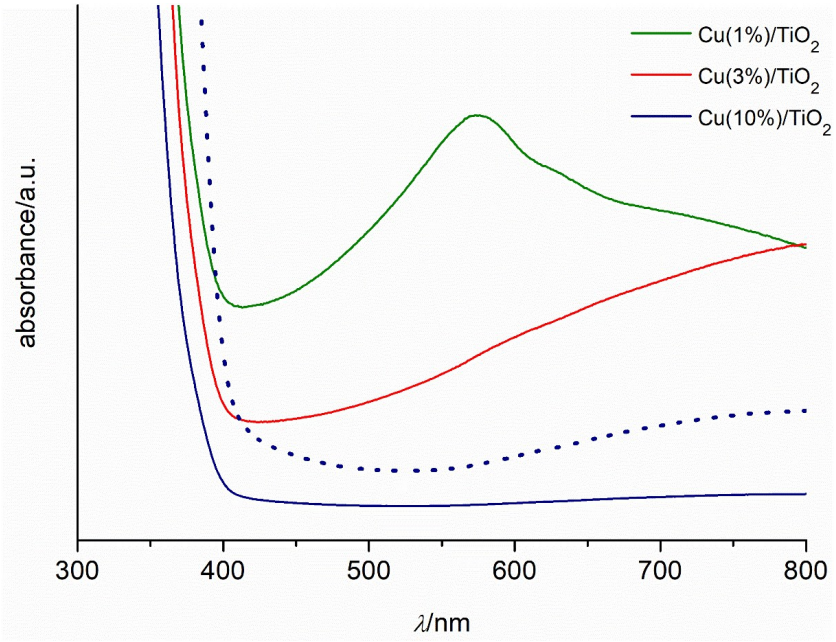

Fig. S3 DRUV-vis spectra of Cu(*X*%)/TiO_2 (*X* = 1, 3 or 10) photocatalysts. The intensity for the sample with lower copper loading (*X* = 1) was increased five-fold (dotted line) in order to clearly observe the weak broad band above 550 nm. This band is significantly more intense for Cu(3%)/TiO_2, whereas the signal corresponding to the localised surface plasmon resonance of Cu(0) nanoparticles (574 nm) is only clearly visible for Cu(10%)/TiO_2.

Table S5 Amounts of gaseous products formed during simulated sunlight irradiation of aqueous acetic acid using Cu/TiO_2 photocatalysts for increasing lengths of time.[a]

photocatalyst	*t*/h	produced amounts/µmol				H_2/CH_4
		H_2	CH_4	CO_2	C_2H_6	
$Cu(1\%)/TiO_2$	1.0	-	46.7	23.6	0.1	-
	2.0	-	85.2	41.0	0.2	-
	4.5	0.02	179.1	89.6	0.7	10^{-4}
	7.0	0.7	195.1	102.9	0.8	$3\ 10^{-3}$
	24	4.8	245.9	126.6	0.9	$2\ 10^{-2}$
$Cu(3\%)/TiO_2$	1.0	-	35.9	17.1	-	-
	2.0	0.1	79.7	39.8	0.3	10^{-3}
	4.5	0.3	166.3	81.5	0.6	$2\ 10^{-3}$
	7.0	0.7	261.7	130.7	1.1	$3\ 10^{-3}$
	24.0	6.6	637.8	319.9	5.4	10^{-2}
$Cu(10\%)/TiO_2$	1.0	-	34.2	16.7	-	-
	2.0	-	71.0	35.2	-	-
	4.5	0.4	167.0	85.0	0.7	$2\ 10^{-3}$
	7.0	0.9	214.1	110.2	1.2	$4\ 10^{-3}$
	24	7.3	656.8	336.7	6.4	10^{-2}
$^{IS}Cu(3\%)/TiO_2$[b]	1.0	1.04	8.51	7.79	0.2	0.12
	2.5	2.33	16.0	12.8	0.3	0.15
	19.0	19.9	126.9	79.6	1.1	0.16

[a] Experimental conditions as described in Table S3. [b] Experimental conditions as described in Section S4.2 for Cu/TiO_2 generated *in situ*.

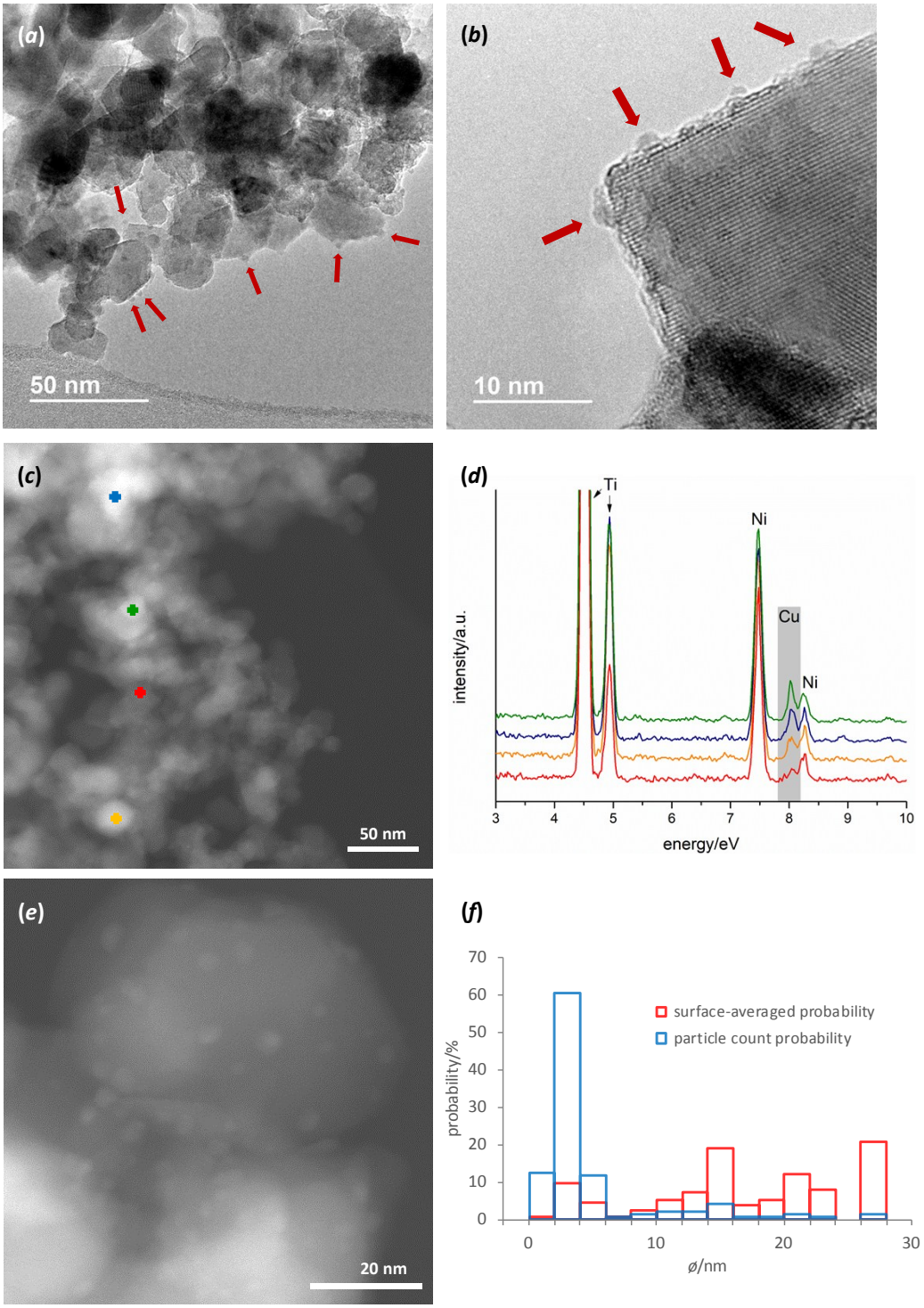

Fig. S4 TEM images and data for Cu(3%)/TiO_2. HRTEM images at × 10^5 and × 5 10^5 magnification (*a* and *b*, respectively) showing the smaller, amorphous, copper nanoparticles (examples marked by arrows) deposited on the larger TiO_2 particles. STEM images at × 5 10^5 and × 2.0 10^6 magnification (*c* and *e*, respectively) showing the presence of copper particles as brighter domains. EDX spectra (*d*) acquired from the spots marked in (*c*) confirmed the presence of copper particles of large sizes (up to ≈ 30 nm, see for example, green spot in *c* and green spectrum in *d*) observed as brighter areas, whereas the less bright areas contain titanium yet smaller amounts of copper (see for example, red spot in *c* and red spectrum in *d*). The particle distribution histogram is represented as histograms both for particle number and surface-averaged probability (*f*).

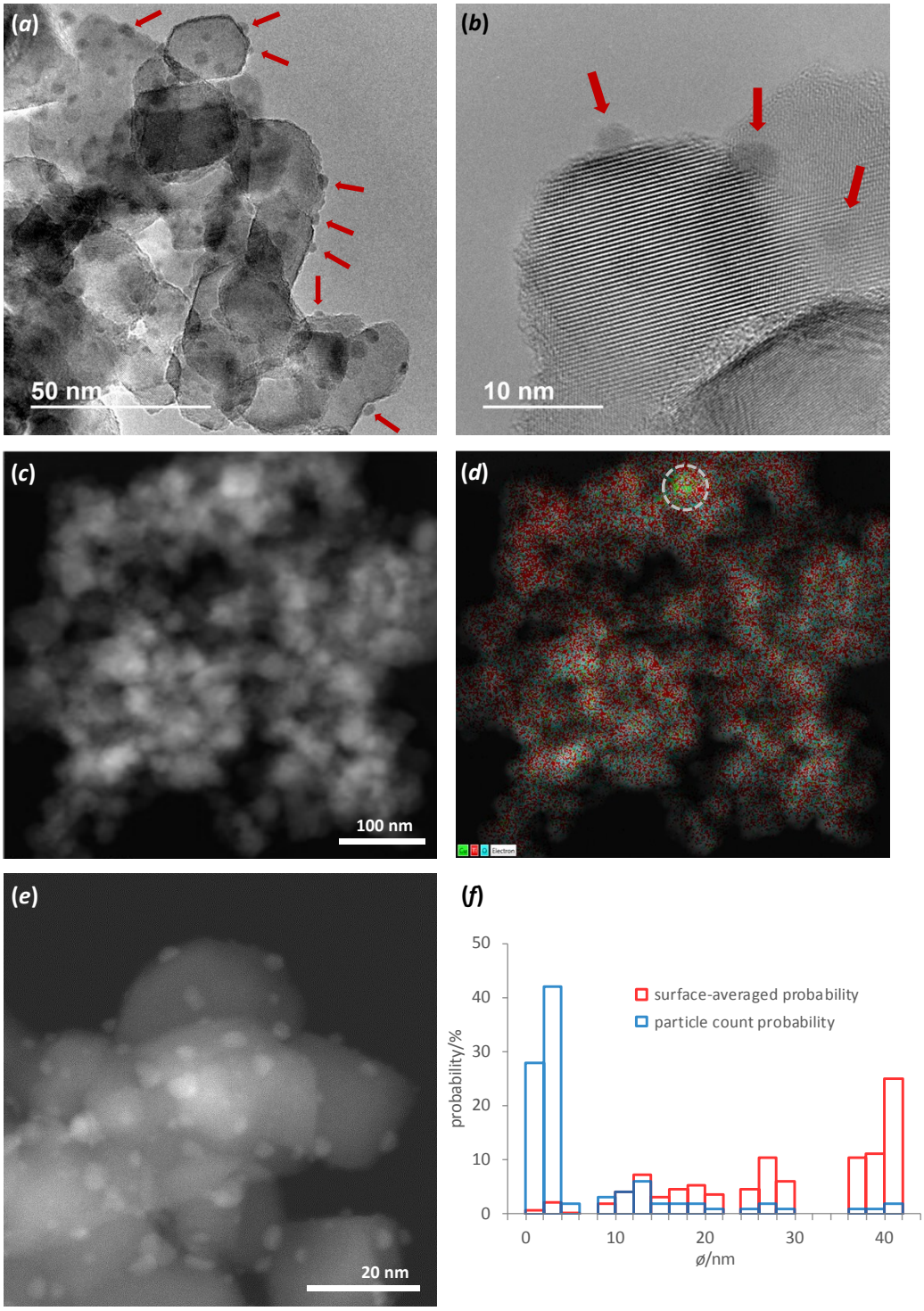

Fig. S5 TEM images and data for Cu(10%)/TiO_2. HRTEM images at × 1.5 10^5 and × 5 10^5 magnification (*a* and *b*, respectively) showing the smaller, amorphous, copper nanoparticles (examples marked by arrows) deposited on the larger TiO_2 particles. STEM images at × 3 10^5 and × 2.0 10^6 magnification (*c* and *e*, respectively) showing the presence of copper particles. Overlaying elemental mapping obtained from EDX data (green, Cu; red, Ti; blue, O; *d*) for the site shown in (*c*) proved that large copper particles (up to ≈ 40 nm, an example marked inside a dotted circle) were also present in the material in addition to the clearly visible smaller ones (for example, in *e*). The particle distribution histogram is represented as histograms both for particle number and surface-averaged probability (*f*).

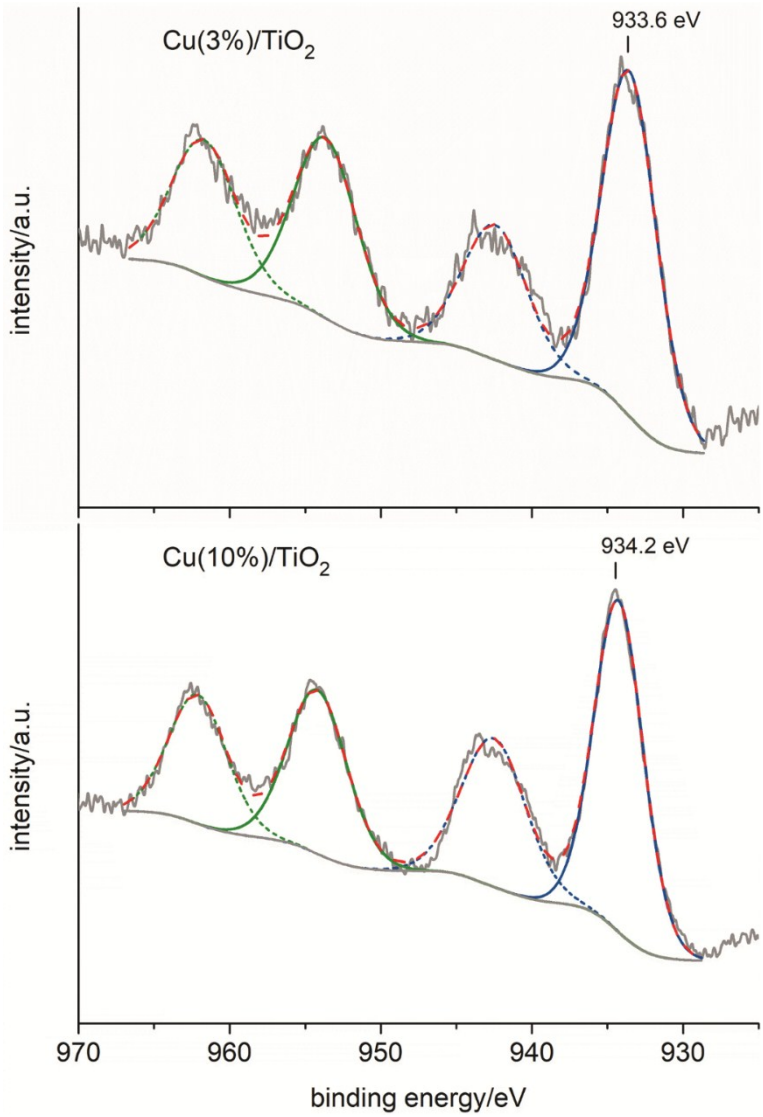

Fig. S6 Raw Cu2p XPS spectra of Cu(3%)/TiO_2 and Cu(10%)/TiO_2 (grey lines), along with the deconvoluted $Cu2p_{3/2}$ and $Cu2p_{1/2}$ components (blue and green lines, respectively), and their corresponding satellite signals (dotted blue and green lines, respectively). The sum of all deconvoluted spectra is represented by a dashed red line, whereas the calculated background is represented by the bottom grey line. Both the presence of the satellite signals, and the position of the $Cu2p_{3/2}$ peaks above 933.5 eV indicate that the oxidation state of copper in surface layers is 2+.

Table S6 Apparent photonic efficiencies (Φ_a) for the transformation of aqueous acetic acid using Cu(3%)/TiO_2 generated *in situ* under monochromatic light, and comparison to literature data. Notwithstanding that direct comparison cannot be made owing to the scarcity of data on closely related photocatalysis, a semi-quantitative evaluation of the data listed below reveals that the photonic efficiencies of our system is comparable to literature data. For example, lower efficiencies were reported for the most similar systems found in the prior art (reference 1) using acetic acid as a substrate—albeit at a lower concentration—and TiO_2—albeit loaded with other metal co-catalysts. Formic acid as a substrate (reference 2) resulted in slightly higher photonic efficiencies—yet the photocatalyst was a sensibly different one, based on CdS. Finally, the use of hydroxyl-containing substrates (references 3–5) has been shown to proceed at notably high photonic efficiencies, due to their propensity to undergo hole-induced oxidation.

photocatalyst	reaction medium	λ/nm	Φ_a/%[a]			reference
			H_2	CH_4	overall	
^{IS}Cu(3%)/TiO_2(P25)[b]	H_2O/CH_3COOH (1:1)	350	1.7	9.2	10.8	this work
Pt(1%)/TiO_2(P25)	CH_3COOH (*aq*, 0.5 M)	365	0.9	1.4	2.3	1
IrO_2(1%)/TiO_2(P25)	CH_3COOH (*aq*, 0.5 M)	365	0.2	1.0	1.2	1
Ru(0.99%)/CdS(21%)/Al-HMS[c]	H_2O/HCOOH (4:1)	420			16.6	2
Pt(5%)/TiO_2(rutile)	H_2O/lactic acid (1:1)	360			71	3
Pt(0.5%)/TiO_2(P25)	glycerol (*aq*, 1 M)	365			71	4
Cu/TiO_2(mesoporous)[d]	CH_3CH_2OH/H_2O (95:5)	?			≈ 50	5

[b] Apparent photonic efficiencies calculated as follows: $\Phi = 100 * [n(e^-)/n(\text{photons})]$, where $n(e^-)$ is the number (moles) of electrons involved in the formation of products, and n(photons) is the number (moles) of incident photons as measured by using a calibrated photodiode. The stoichiometries of the most likely reactions, including the participating electrons/holes, are as follows:

1) $CH_3COOH + h^+ + e^- \rightarrow CH_4 + CO_2$
2) $2\ CH_3COOH + 2\ h^+ + 2\ e^- \rightarrow C_2H_6 + H_2 + CO_2$
3) $CH_3COOH + H_2O + 2\ h^+ + 2\ e^- \rightarrow CH_3OH + H_2 + CO_2$
4) $CH_3COOH + H_2O + 4\ h^+ + 4\ e^- \rightarrow HCHO + 2\ H_2 + CO_2$
5) $CH_3COOH + 2\ H_2O + 6\ h^+ + 6\ e^- \rightarrow HCOOH + 3\ H_2 + CO_2$
6) $CH_3COOH + 2\ H_2O + 8\ h^+ + 8\ e^- \rightarrow 4\ H_2 + 2\ CO_2$

from which the electron-to-product ratios are determined as follows: $[n(e^-)/n(CH_4)] = 1$ (reaction 1); and $[n(e^-)/n(H_2)] = 2$ (reactions 2–6).

[a] Experimental conditions as described in Section S4.2; reaction time: 1 h.

[c] HMS: hexagonal mesoporous silica.

[d] Uncertain amount of copper deposited *in situ* under Hg lamp (1000 W) light irradiation.

References:

1 S. Hamid, *PhD Thesis*, Leibniz Universität Hannover, 2018.
2 Y.J. Zhang, L. Zhang and S. Li, *Int. J. Hydrogen Energy*, 2010, 35, 438-444.
3 H. Harada, T. Ueda and T. Sakata, *J. Phys. Chem.*, 1989, 93, 1542-1548.
4 D.I. Kondarides, V.M. Daskalaki, A. Patsoura and X.E. Verykios, *Catal. Lett.*, 2008, 122, 26-32.
5 A.V. Korzhak, N.I. Ermokhina, A.L. Stroyuk, V.K. Bukhtiyarov, A.E. Raevskaya, V.I. Litvin, S.Y. Kuchmiy, V.G. Ilyin and P.A. Manorik, *J. Photochem. Photobiol. A-Chem.*, 2008, 198, 126-134.

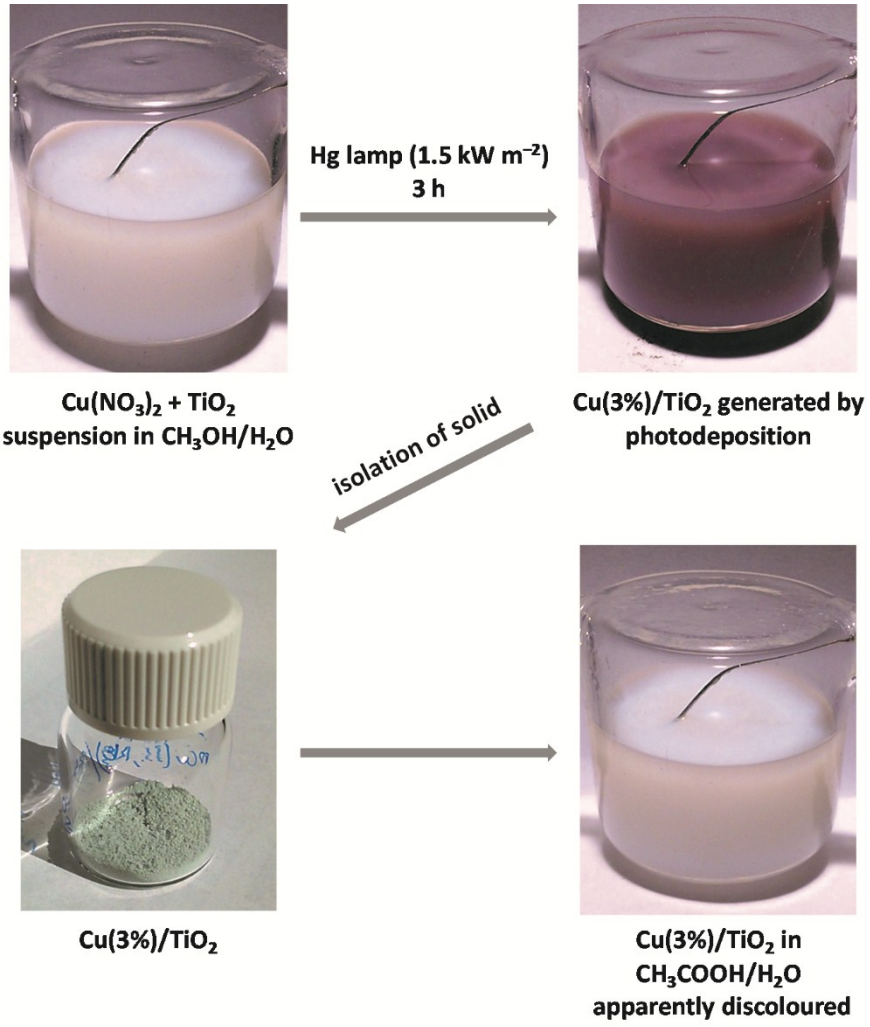

Fig. S7 Pictures illustrating the colour differences indicative of changes in copper oxidation states. Photodeposition causes colour change from an initial off-white for the suspension containing TiO_2 and the Cu^{2+} precursor salt (top left) to an intense purple-pink colouration (top right) consistent with the surface plasmon resonance absorption of deposited Cu(0) nanoparticles. The isolated Cu(3%)/TiO_2 solid changed into a pale blue colouration (bottom left), most likely due to re-oxidation of copper in air (see main text for details). Dispersion of Cu(3%)/TiO_2 in CH_3COOH/H_2O resulted in an off-white suspension (bottom right).

Table S7 Amounts of gaseous products formed during redox cycling experiments by simulated sunlight irradiation of aqueous acetic acid using Cu(3%)/TiO_2 photocatalysts.[a]

cycle	*t*/h	produced amounts/µmol				H_2/CH_4
		H_2	CH_4	CO_2	C_2H_6	
	conventional photocatalyst, air-oxidised					
#*ox1*	1.0	0.01	30.7	16.4	0.1	$2\ 10^{-4}$
	2.0	0.02	57.0	30.3	0.1	$6\ 10^{-3}$
	3.0	0.02	85.5	45.9	0.2	$2\ 10^{-4}$
	photoreduction					
#*red1*	1.0	0.30	11.3	9.6	0.2	0.03
	2.0	0.75	16.9	13.9	0.3	0.04
	3.0	1.17	20.5	16.2	0.3	0.06
	air oxidation					
#*ox2*	1.0	0.02	24.1	14.0	0.2	$8\ 10^{-4}$
	2.0	0.05	48.8	27.7	0.2	10^{-3}
	3.0	0.11	68.6	39.4	0.3	$2\ 10^{-3}$
	photoreduction					
#*red2*	1.0	0.40	4.9	5.0	0.2	0.08
	2.0	0.82	8.5	7.1	0.2	0.10
	3.0	1.32	12.7	9.7	0.2	0.10

[a] Experimental conditions as described in Table S3 and the redox cycling procedure in Section S4.4.